International Journal of High-Rise Buildings
www.ctbuh-korea.org/ijhrb/index.php

International Journal of High-Rise Buildings
December 2022, Vol 11, No 4, 315-320
https://doi.org/10.21022/IJHRB.2022.11.4.315

Multi-objective Optimization of Pedestrian Wind Comfort and Natural Ventilation in a Residential Area

H.Y. Peng, S.F. Dai, D. Hu, and H.J. Liu†

School of Civil and Environmental Engineering, Harbin Institute of Technology, Shenzhen, China

Abstract With the rapid development of urbanization the problems of pedestrian-level wind comfort and natural ventilation of tall buildings are becoming increasingly prominent. The velocity at the pedestrian level ($\overline{MVR}$) and variation of wind pressure coefficients $\overline{\Delta C_p}$ between windward and leeward surfaces of tall buildings were investigated systematically through numerical simulations. The examined parameters included building density ρ, height ratio of building α_H, width ratio of building α_B, and wind direction θ. The linear and quadratic regression analyses of $\overline{MVR}$ and $\overline{\Delta C_p}$ were conducted. The quadratic regression had better performance in predicting $\overline{MVR}$ and $\overline{\Delta C_p}$ than the linear regression. $\overline{MVR}$ and $\overline{\Delta C_p}$ were optimized by the NSGA-Ⅱ algorithm. The LINMAP and TOPSIS decision-making methods demonstrated better capability than the Shannon's entropy approach. The final optimal design parameters of buildings were ρ = 20%, α_H = 4.5, and α_B = 1, and the wind direction was θ = 10°. The proposed method could be used for the optimization of pedestrian-level wind comfort and natural ventilation in a residential area.

Keywords CFD, pedestrian-level wind comfort, natural ventilation, multi-objective optimization

†Corresponding author:
H.J. Liu
Tel: +8675526033805
E-mail:
liuhongjun@hit.edu.cn

1. Introduction

With the increase in population growth and urbanization, the pedestrian-level comfort and natural ventilation have attracted more and more attention. Good wind conditions provide people with comfort in outdoor and indoor spaces (Abdel-Ghany et al., 2013; Lai et al., 2014). Urban environments are affected by building parameters, building configurations, and approaching flow (Wu and Niu, 2017; Liu and Niu, 2019). To improve the urban wind environments, multi-objective optimization of the pedestrian-level comfort and natural ventilation should be conducted.

Yim et al. (2009) performed computational fluid dynamics (CFD) simulations to investigate the interference effect of an upwind building on wind conditions at the pedestrian height around the downward building. The velocity at the pedestrian height around the principal building was significantly reduced due to the shielding effect of the upstream interfering building. Tsang et al. (2012) studied the pedestrian-level wind environment in the area with different building configurations by wind tunnel tests. A wider building configuration improved the pedestrian-level comfort due to the reduction of areas with large velocities. Zhang et al. (2005) examined the effect of building arrangement on the flow fields around buildings via CFD simulations. A special building arrangement was proposed to improve the quality of natural ventilation. An innovative and creative passive element was added to improve the natural ventilation of the building (Shaeri et al., 2022). The pedestrian-level wind environment and natural ventilation were investigated in the literature. Nevertheless, the effects of design parameters of buildings on the pedestrian-level comfort and natural ventilation were not jointly examined.

Du et al. (2018) investigated the optimization scheme of pedestrian-level wind condition around an isolated building with lift-up design through CFD simulations and the response surface methodology (RSM) technique. A multi-variable optimization method was proposed to achieve the high-level pedestrian comfort. Zhang et al. (2018) studied the effects of some important design parameters on the wind comfort around a lift-up building in the wind tunnel. A non-linear second-order multivariable regression model was employed to predict the velocity at the pedestrian height around the lift-up building. The literature has reported the optimization of velocity at pedestrian height. However, the multi-objective optimization of both the pedestrian-level comfort and natural ventilation was less studied.

In this study, the velocity at the pedestrian level and the variation of wind pressure coefficients between windward and leeward surfaces of buildings were studied via CFD

simulations. The examined parameters included building density ρ, height ratio of building α_H, width ratio of building α_B, and wind direction θ. Besides, regression analyses of velocity ratios and variations of wind pressure coefficients with various parameters were conducted. The genetic algorithm of NSGA-II was utilized to carry out the multi-objective optimization.

2. CFD Validation

2.1. Description of the case for validation

In this study, the case of an idealized building array (AIJ, 2016) was selected. The experimental results from the benchmark wind tunnel tests in the AIJ guideline (AIJ, 2016) were used for the validation of CFD simulations in this study. As shown in Figure 1(a), the principal building (marked by red color) was surrounded by eight buildings. The dimensions of all nine cubic buildings were the same, and the side length was 0.2 m at the model scale. The spacing between the adjacent buildings was 0.2 m. Furthermore, 120 measurement points were set around the principal building. Figure 1(b) shows the normalized mean wind velocity and its fluctuating counterpart profiles. Note that the velocity fluctuation referred to the ratio of the root-mean-square value of velocity to the mean velocity at the reference height (0.1 m above the ground). Detailed experimental setup and inflow boundary conditions can be referred to the literature (AIJ, 2016).

2.2. Numerical set-up

The computational domain was shown in Figure 2, where 3 × 3 arrayed buildings were set to be consistent with AIJ guideline (AIJ, 2016) for validation. The dimensions of the computational domain were set based on the literature (Franke et al., 2007; Tominaga et al., 2008). The upstream and downstream domain distances were 5H (450 m) and 15H (1350 m), respectively, where

Table 1. Boundary conditions

Boundary	Setup
Inlet	$\varepsilon = C_\mu^{0.5} k \frac{du}{dz}$, $\omega = \frac{\varepsilon}{C_\mu k}$, $C_\mu = 0.09$
Outlet	Outflow
Top and Side	Symmetry
Ground	Wall with z_o = 0.42 m
Interface-out and -in	Interface
Building surface	Wall with z_o = 0

H is the height of the highest building among all studied cases (H = 90 m). The height of the domain was 7H (630 m). The maximum blockage ratio was less than 3.0%, satisfying the requirements (Franke et al., 2007; Tominaga et al., 2008). The boundary conditions were listed in Table 1.

The y+ values ranged from 30 to 600, satisfying the requirement of proper near-wall mesh quality by the standard wall functions (Yang et al., 2016; Wang et al., 2017). The grid growth rate was approximately 2.0. ANSYS Fluent was used as the CFD solver and convergence was assumed when all scaled residuals reached 10^{-6}.

The width and length of the studied area were 150 m and 160 m at full scale, respectively. The depth D of buildings was kept as 20 m, whereas the widths B of buildings were 30 m, 40 m, and 60 m. Furthermore, the width and length of the residential area were 150 m and 160 m, respectively. The heights of buildings were 30 m, 45 m, 60 m, 75 m, and 90 m, respectively. The building density was defined as the ratio of the planned areas of buildings to the residential area ($\rho = S_B/S_R$, S_B and S_R are the planned areas of buildings and the residential area, respectively). Hence, the building densities were 10%, 20%, 30%, and 40%. At each width ratio, i.e., B/D = 1.5, 2.0 and 3.0, four kinds of building densities, i.e., ρ = 10%, 20%, 30%, and 40%, were studied. For building density

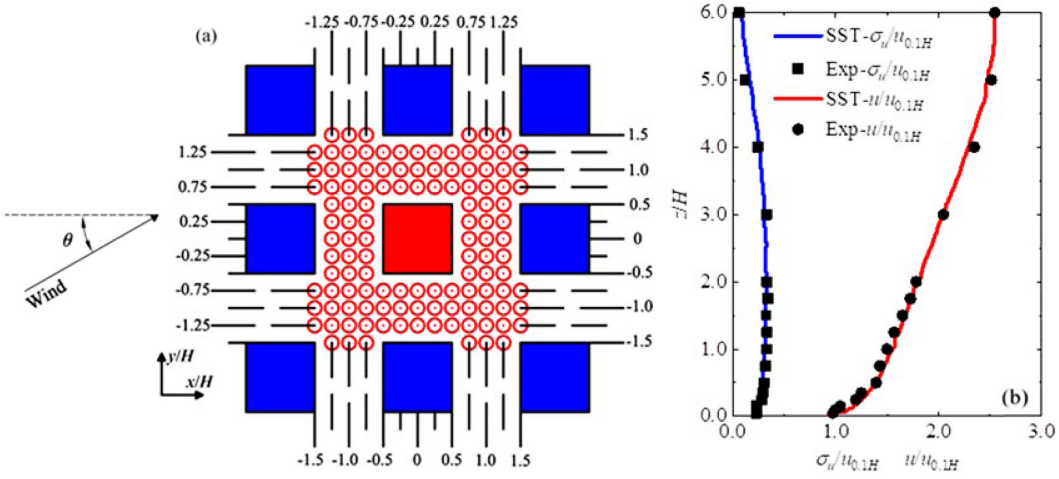

Figure 1. (a) Diagram of measurement points (plan view) and (b) wind profile of wind tunnel tests (AIJ, 2016).

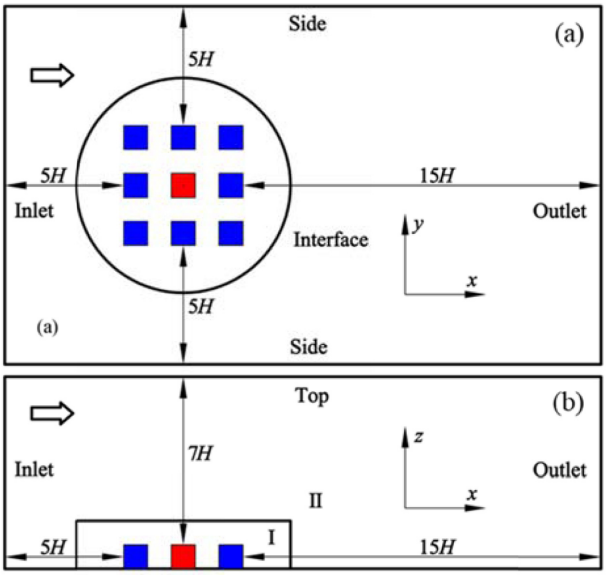

Figure 2. Computational domain: (a) side view and (b) top view.

of 10%, buildings are equally spaced in one column along the direction perpendicular to the zero wind direction at the center. Similarly, at ρ = 20%, 30%, and 40%, there are 2, 3, and 4 columns of equally spaced buildings, respectively. The various building densities were related to numbers of buildings in the area. Given the symmetrical geometry of the buildings and measurement points, the simulations were conducted at five different wind directions (θ = 0°, 22.5°, 45°, 67.5°, and 90°).

2.3. Grid-independence analysis

The velocity ratio *VR* was used to evaluate the wind comfort at the pedestrian level (2 m above the ground), as indicated in Equation (1).

$$VR = \frac{u}{u_0} \tag{1}$$

where u and u_0 were velocities at the height of 2.0 m above the ground in the disturbed (with buildings) and undisturbed (without buildings) flows, respectively.

The variations of wind pressure coefficients ΔC_p on the windward and leeward faces of buildings were employed to assess the natural ventilation potential of buildings (Esfeh et al., 2021; Jiang et al., 2022). Large ΔC_p would induce high wind velocities through buildings and thereby enhance the natural ventilation, whereas small ΔC_p would reduce the performance of natural ventilation.

$$\Delta C_p = \frac{P_w - P_l}{0.5\rho U_{ref}} \tag{2}$$

where P_w was wind pressure on the windward surfaces of buildings, P_l was wind pressure on the leeward surfaces of buildings, ρ was the air density, and U_{ref} was velocity at the roof height.

Three grid schemes were adopted to examine the grid sensitivity. The smallest sizes of the three sets of grids were 0.06 m (coarse), 0.03 m (basic), and 0.015 m (fine) (Anbarsooz and Amiri, 2022; Dai et al., 2022). The coarse grid had 1.4 million cells, the basic grid had 2.93 million cells, and the fine grid had 6.05 million cells, satisfying the requirement according to Zheng et al. (2020). The three sets of grids are displayed in Figure 3.

Figure 4 compares *VR* in the *y*-*z* plane at x = 0 among the three grid schemes. The results showed that the variations of *VR* between the coarse and basic grids were

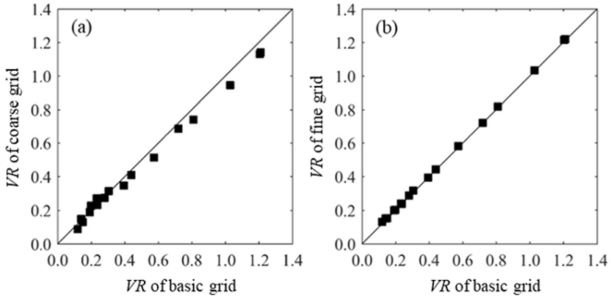

Figure 4. Comparison of VR between grid schemes: (a) coarse and basic grids and (b) basic and fine grids.

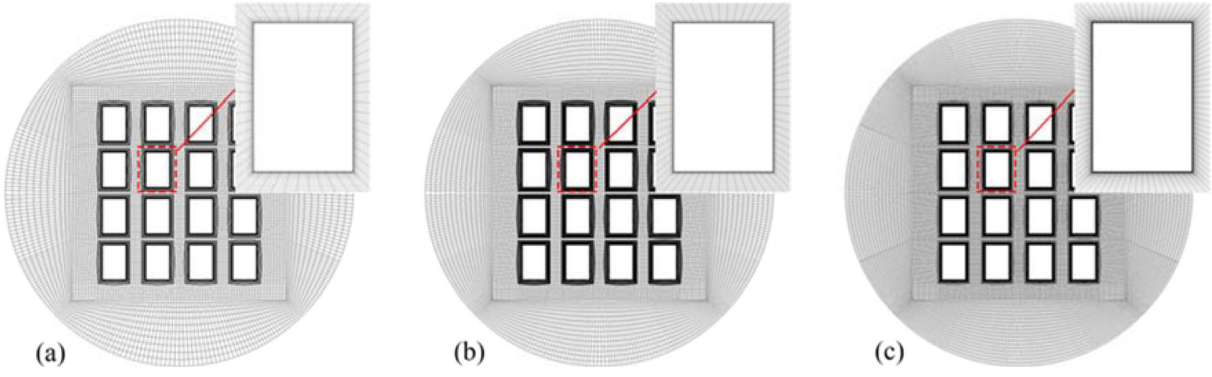

Figure 3. Mesh details of three set of grids: (a) coarse, (b) minimum, and (c) fine.

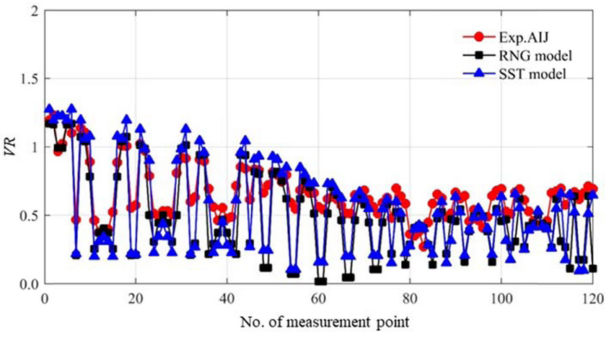

Figure 5. Comparison of *VR* between CFD simulation and experimental results (AIJ, 2016).

large (see Figure 4(a)). However, the basic and the fines grids showed similar results (see Figure 4(b)). Considering the balance between the computational cost and prediction accuracy, the basic grid (2.9 million cells) was chosen for numerical simulations.

2.4. Validation results

To validate the CFD methodology, the prediction results were compared with the experimental data (AIJ, 2016). Figure 5 compared *VR* of 120 points (see Figure 1) calculated by the SST k–ω (Menter, 1994) and RNG k–ε (Yakhot and Orszag, 1986) turbulence models with the test results (AIJ, 2016). Both the SST and RNG models agreed well with the experimental results for large *VR*, whereas they slightly underestimated *VR* for small *VR*. The underestimation of *VR* is attributed to that the RANS models might not be able to properly reproduce the complex flows at the rear regions of buildings. In general, the SST model showed good performance to predict *VR* around buildings compared with the RNG model. Hence, the numerical simulations were conducted by the SST model.

3. Results and discussion

3.1. Prediction models of pedestrian-level comfort and natural ventilation

The area-weighted $\overline{MVR}$ was defined to assess the wind comfort at pedestrian level in the entire area.

$$\overline{MVR} = \frac{\int VR dA}{A} \tag{3}$$

where A was the area. The mean variation of wind pressure coefficients between windward and leeward surfaces was defined to evaluate the natural ventilation as follows:

$$\Delta C_p = \frac{\sum_{i=1}^{n} \Delta C_P(i)}{n} \tag{4}$$

where $\Delta C_p(i)$ was the variation of wind pressure on the surfaces of the ith building, and n was the number of buildings in the studied area.

The quadratic regressions of $\overline{MVR}$ and $\overline{\Delta C_p}$ with various parameters could be obtained as follows:

$$\begin{aligned}\overline{MVR} = {} & \\ & 1.001 - 3.243\gamma + 0.064\alpha_B + 0.029\sin\theta - 0.655\cos\theta \\ & + 1.789\gamma\sin\theta + 3.001\gamma\cos\theta\end{aligned} \tag{5}$$

$$\begin{aligned}\overline{\Delta C_p} = {} & \\ & -0.092 - 0.569\cos\theta - 1.005\gamma\cos\theta + 0.025\alpha_H + 0.73\sin\theta\end{aligned} \tag{6}$$

where γ was the building density, α_H was the building height ratio, α_B was the building width ratio, and θ was the wind direction.

Figure 6 shows the linear (first-order) and quadratic (second-order) regression of $\overline{MVR}$ and $\overline{\Delta C_p}$ with various parameters. Observations showed that the linear model encountered underestimations of $\overline{\Delta C_p}$ larger than 0.3 (see Figure 6(c)). The quadratic regression performed well in predicting both $\overline{MVR}$ and $\overline{\Delta C_p}$ compared with the linear regression. Hence, the quadratic models could be applied for the estimation of pedestrian wind environment and natural ventilation in building areas.

3.2. Multi-objective optimization

There are multiple solutions for multi-objective optimization problems. The optimization objective functions are normally constrained by each other, inducing that the optimal solutions cannot be achieved at the same time.

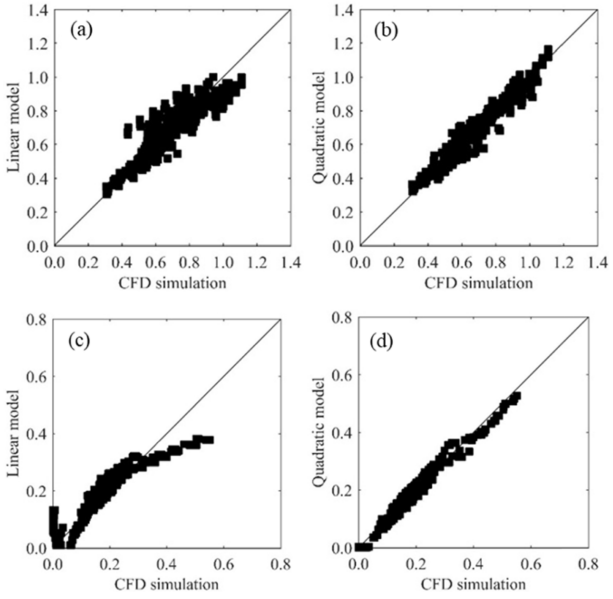

Figure 6. The linear and quadratic regressions of $\overline{MVR}$ and $\overline{\Delta C_p}$: (a) linear for $\overline{MVR}$, (b) quadratic for $\overline{MVR}$, (c) linear for $\overline{\Delta C_p}$, and (d) quadratic for $\overline{\Delta C_p}$.

Table 2. Parameters used in the NSGA-II algorithm

Parameter	Value
Population size	150
Maximum generation	500
Tournament size	10
Crossover probability	0.9
Mutation probability	0.1
Pareto fraction	0.6

Table 3. Ranges of parameters for optimization

Parameter	Range
Building density ρ	(0, 50%]
Height ratio α_H	[1, 5]
Width ratio α_B	[1, 5]
Wind direction θ	(0, 180°]

For multi-objective optimization problem, the Pareto optimal front can be calculated by the genetic algorithm of NSGA-II (Srinivas and Deb, 1994; Deb, 2001), with good robustness and convergence. The set of optimal solutions by NSGA-II are named as the Pareto optimal front.

Smaller $\overline{MVR}$ suggests better wind comfort at the pedestrian level and larger $\overline{\Delta C_p}$ means higher quality of natural ventilation. Nevertheless, the optimal pedestrian wind comfort and natural ventilation cannot be achieved simultaneously. The multi-objective NSGA-II was employed to obtain the Pareto optimal front of $\overline{MVR}$ and $\overline{\Delta C_p}$. The setting parameters of NSGA-II algorithm are listed in Table 2 and the ranges of parameters for optimization are listed in Table 3.

3.3. Optimum results

The optimization method in this study was a genetic algorithm-based optimization technology based on genetic algorithm and decision-making. This method could optimize multiple design variables and multiple objectives. The optimization method had three stages: (1) to develop a surrogate model for optimization, (2) to implement the multi-objective optimization process, and (3) to conduct the decision-making scheme. In doing this, the optimization for pedestrian-level wind comfort and natural ventilation of buildings could be accomplished in a systematic way.

In Section 3.2, the Pareto optimal front of $\overline{MVR}$ and $\overline{\Delta C_p}$ was obtained and were plotted by red dots in Figure 7. To determine the optimal solutions, three decision-making methods (LINMAP (Yu, 1985; Olson, 1996), TOPSIS (Hwang and Yoon, 1981; Yu, 1985; Olson, 1996), and Shannon's entropy (Guisado et al., 2005)) were employed. As shown in Figure 7, the blue dots represent the non-ideal and ideal solutions, while the black dots at the pareto optimal front denote the final optimum solutions achieved by LINMAP, TOPSIS, and Shannon's entropy methods.

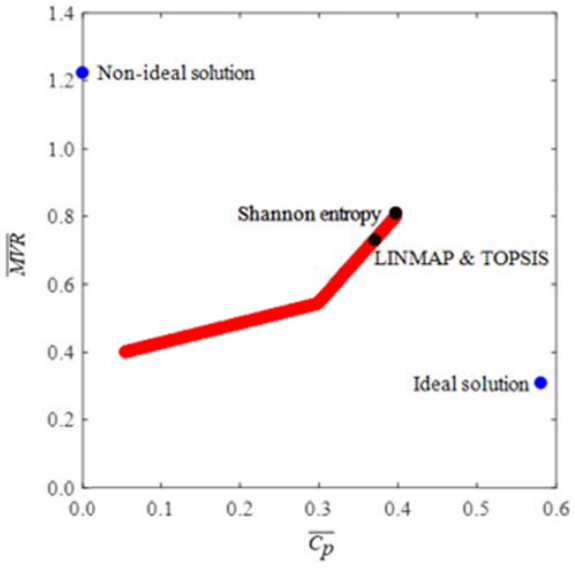

Figure 7. The Pareto optimal front by the three decision-making methods.

To select a final optimum solution, the deviation value s (Du et al., 2019) was calculated. The values of s for the LINMAP, TOPSIS, and Shannon's entropy methods were 0.508, 0.508, and 0.721, respectively. Therefore, the results from LINMAP and TOPSIS methods gave the final solution. $\overline{MVR}$ and $\overline{\Delta C_p}$ were 0.68 and 0.39, respectively. The optimal parametric settings were $\rho = 20\%$, $\alpha_H = 4.5$, $\alpha_B = 1.0$, and $\theta = 10°$.

4. Conclusions

The linear and quadratic regression analyses for $\overline{MVR}$ and $\overline{\Delta C_p}$ were conducted. The quadratic regression performed well for both $\overline{MVR}$ and $\overline{\Delta C_p}$ compared with the linear regression. The relationships between $\overline{MVR}$ and $\overline{\Delta C_p}$ with the various parameters were examined. Those regression models could be used to assess the pedestrian-level wind comfort and natural ventilation in residential areas.

The LINMAP, TOPSIS, and Shannon's entropy were used to determine the final optimal solutions. The results showed that the LINMAP and TOPSIS approaches did a better work than the Shannon's entropy method. The optimal $\overline{MVR}$ and $\overline{\Delta C_p}$ were 0.68 and 0.39, respectively. The optimal parameters were $\rho = 20\%$, $\alpha_H = 4.5$, $\alpha_B = 1$, and $\theta = 10°$. The proposed multi-objective optimization method could be employed to optimize the design parameters of residential buildings for optimal pedestrian-level comfort and natural ventilation.

Acknowledgments

This work was supported by National Natural Science Foundation of China (Grant No.: 51978221), Shenzhen

Science and Technology Innovation Committee (Grant No.: GXWD20201230155427003-20200824100128002) and Characteristic and Innovation Projects of Universities in Guangdong Province (Grant No.: 2021KTSCX367). The authors would like to express their gratitude for the support.

References

Abdel-Ghany, A.M., Al-Helal, I.M., and Shady, M.R. (2013). "Human thermal comfort and heat stress in an outdoor urban arid environment: a case study." Advances in Meteorology, 693541.

AIJ (2016). "Benchmark tests of flow around building group models. In: Architectural Institute of Japan AIJ Benchmarks for Validation of CFD Simulations Applied to Pedestrian Wind Environment Around Buildings." Architectural Institute of Japan, Tokyo, 56-65.

Anbarsooz, M., Amirii, M. (2022). "Towards enhancing the wind energy potential at the built environment: Geometry effects of two adjacent buildings." Energy, 239, 122351.

Deb, K. (2009). "Multi-objective optimisation using evolutionary algorithms: An introduction." Springer.

Dai, S.F., Liu, H.J., and Peng, H.Y. (2022). "Assessment of parapet effect on wind flow properties and wind energy potential over roofs of tall buildings." Renewable Energy, 199, 826-839.

Du, Y., Mak, C.M., and Li, Y. (2018). "Application of a multi-variable optimization method to determine lift-up design for optimum wind comfort." Building and Environment, 131, 242-254.

Du Y., Mak C.M., Li Y. (2019). "A Multi-Stage Optimization of Pedestrian Level Wind Environment and Thermal Comfort with Lift-Up Design in Ideal Urban Canyons." Sustainable Cities and Society, 46, 56-63.

Esfeh, M.K., Sohankar, A., Shahsavari, A.R., Rastan, M.R., Ghodrat, M., and Nili, M. (2021). "Experimental and numerical evaluation of wind-driven natural ventilation of a curved roof for various wind angles." Building and Environment, 205, 108275.

Franke, J., Hellsten, A., Schlünzen, H., and Carissimo, B. (2007). Best practice guideline for the CFD simulation of flows in the urban environment. COST Action 732, 1-52.

Guisado J.L., Jiménez-Morales F., and Guerra J.M. (2005). "Application of Shannon's Entropy to Classify Emergent Behaviors in a Simulation of Laser Dynamics." Mathematical and Computer Modelling, 42, 847-854.

Jiang, Z., Kobayashi, T., Yamanaka, T., Sandberg, M., Kobayashi, N., Choi, N., and Sano, K. (2022). "Validity of Orifice equation and impact of building parameters on wind-induced natural ventilation rates with minute mean wind pressure difference." Building and Environment, 219, 109248.

Lai, D., Guo, D., Hou, Y., Lin, C., and Chen, Q. (2014). "Studies of outdoor thermal comfort in northern China." Building and Environment, 77, 110-118.

Liu, J., and Niu, J. (2019). "Delayed detached eddy simulation of pedestrian-level wind around a building array-The potential to save computing resources." Building and Environment, 152, 28-38.

Menter F.R. (1994). "Two-equation eddy-viscosity turbulence models for engineering applications." AIAA Journal, 32, 1598-1605.

Olson D.L. (1996). "Decision Aids for selection problems." New York: Springer.

Shaeri, J., Mahdavinejad, M., and Pourghasemian, M.H. (2022). "A new design to create natural ventilation in buildings: Wind chimney." Journal of Building Engineering, 105041.

Tsang, C.W., Kwok, K.C.S., and Hitchcock, P.A. (2012). "Wind tunnel study of pedestrian level wind environment around tall buildings: Effects of building dimensions, separation and podium." Building and Environment, 49, 167-181.

Srinivas N., Deb K. (1994). "Multiobjective optimization using nondominated sorting in genetic algorithms." Evolutionary Computation, 2, 221-248.

Tominaga, Y., Mochida, A., Yoshie, R., Kataoka, H., Nozu, T., Yoshikawa, M., and Shirasawa, T. (2008). "AIJ guidelines for practical applications of CFD to pedestrian wind environment around buildings." Journal of Wind Engineering and Industrial Aerodynamics, 96, 1749-1761.

Wang, B., Cot, L.D., Adolphe, L., and Geoffroy, S. (2017). "Estimation of wind energy of a building with canopy roof." Sustainable Cities and Society, 35, 402-416.

Wu, Y., and Niu, J. (2017). "Numerical study of inter-building dispersion in residential environments: prediction methods evaluation and infectious risk assessment." Building and Environment, 115, 199-214.

Yakhot V. and Orszag S.A. (1986). "Renormalization group analysis of turbulence I. Basic theory." Journal of Scientific Computing, 57, 1722-1724.

Yang, A.S., Su, Y.M., Wen, C.Y., Juan, Y.H., Wang, W.S., and Cheng, C.H. (2016). "Estimation of wind power generation in dense urban area." Applied Energy, 171, 213-230.

Yu P.L. (1985). "Multiple-Criteria decision making, concepts, Techniques, and Extensions." New York: Plenum Press.

Yoshie, R., Mochida, A., Tominaga, Y., Kataoka, H., Harimoto, K., and Nozu, T., Shirasawa, T. (2007). "Cooperative Project for CFD Prediction of Pedestrian Wind Environment in the Architectural Institute of Japan." Journal of Wind Engineering and Industrial Aerodynamics, 95(9), 1551-1578.

Yim, S.H.L., Fung, J.C.H., Lau, A.K.H., and Kot, S.C. (2009). "Air Ventilation Impacts of the 'Wall Effect' Resulting from the Alignment of High-Rise Buildings." Atmospheric Environment, 43(32), 4982-4994.

Zhang, A., Gao, C., and Zhang, L. (2005). "Numerical simulation of the wind field around different building arrangements." Journal of Wind Engineering and Industrial Aerodynamics, 93(12), 891-904.

Zhang, X., Tse, K.T., Weerasuriya, A.U., Kwok, K.C.S., Niu, J., Lin, L., and Mak, C.M. (2018). "Pedestrian-level wind conditions in the space underneath lift-up buildings." Journal of Wind Engineering and Industrial Aerodynamics, 179, 58-69.

Zheng, X., Montazeri, H., and Blocken, B. (2020). "CFD simulations of wind flow and mean surface pressure for buildings with balconies: Comparison of RANS and LES." Building and Environment, 173, 106747.